Biophysical Journal, Volume 99

Supporting Material

Localization microscopy reveals expression-dependent parameters of chromatin nanostructure

Bohn, Philipp Diesinger, Rainer Kaufmann, Yanina Weiland, Patrick Müller, Manuel Gunkel, Alexa von Ketteler, Paul Lemmer, Michael Hausmann, Dieter W. Heermann, and Christoph Cremer

Supplementary Information

Supplementary Information 1: Noise repression via Voronoi tesselation

As mentioned previously, the experimental raw data was analyzed with two different independent approaches: The previously described density analysis and a method that uses noise repression by Voronoi tesselation. The latter one will be described in the following. Although the two approaches are very different they independently from one another lead to very similar results. In this section the Voronoi tessellation approach to eliminate unwanted background signals inside the fibroblasts or HeLa nuclei is described. Fig. 1A in the manuscript file shows some raw data i.e. the xy-coordinates of the labeled nucleosomes in the case of a Fibroblast nucleus.

If a set of two-dimensional coordinates is given, a Voronoi cell can be constructed for each of these points. If r is one of the given points, then the corresponding cell C_r will consist of all points in the xy-plane that are closer to r than to any other data point. The *segments* of a Voronoi tessellation are the points that are equidistant to two of the given points. Fig. 1 shows such a Voronoi tessellation for some random coordinates.

The Voronoi tessellation has some very useful properties: Its dual graph corresponds to the Delaunay triangulation of the same set coordinates and points are adjacent on the convex hull if and only if their Voronoi cells share an infinitely long segment. A Voronoi tessellation can be used to solve many frequent geometrical problems like the next neighbor problem (resp. the *all* next neighbors problem) and the largest free sphere problem. Furthermore, Voronoi diagrams are used for the analysis of protein structures [4] and many other problems [5].

The size of a Voronoi cell can be calculated easily with the Gaussian trapeze formula that describes the area of a polygon:

$$A = \frac{1}{2}\left|\sum_{i=1}^{n}(y_i + y_{i+1})(x_i - x_{i+1})\right|.$$

The Voronoi tessellation was calculated with the Qhull algorithm [7] in this work by performing a Delauney triangulation first.

For every localization image first a Voronoi diagram was generated (cf. Fig. 1) in order to eliminate the background noise of the raw data. One can see that points which lie in areas which have a very low density have large Voronoi cells.

The large scale density fluctuations in the localization data come from regions which were occupied during the capture time for instance by the nucleoli. Therefore, the number of data points in the final projection image is smaller in these regions. These data points are not used in the following block analysis.

Furthermore, one can also see that some data points lie even outside the cell nucleus. They are not of interest here and will be sorted out as well.

After the generation of the Voronoi tessellation all data points the Voronoi cell size of which is larger than a given cut-off value were taken away. This process is repeated iteratively until the convex hull of the nucleus is unveiled. During these calculations the interior of the nucleus is not changed at all.

The iterative process gives us the advantage that data points which are close to each other (i.e. points with small Voronoi cell sizes) are not changed at all, whereas single abandoned points are taken away. Fig. 2 shows an example of the convex hull determination in the case of a fibroblast nucleus.

After the determination of the nucleus's convex hull the same iterative selection due to Voronoi cell size is done with the data points that lie inside the nucleus (cf. Fig. 2). The two steps are independent of each other to have the possibility of applying different cut-off criteria to the exterior and the interior.

With this method the fluorescent markers which are associated with the heterochromatin are sorted out, too. In the following block analysis only euchromatin shall be considered.

At the end of the described process one gets a noise reduced localization image (cf. Fig. 2).

Block Analysis

For the nanostructure investigation of the data several steps have to be carried out. For every data point of a given nucleus first a square with edge length 800 nm that is centered around that very data point is cut out. Then the mean particle density of that square is calculated.

If the particle density is equal or larger than the the mean particle density of the nucleus, then a circle of radius 400 nm around the considered data point in the center is cut out. Now, if this circle fulfils the same condition i.e. that its mean particle density is equal or larger than the average density of the nucleus, then all distances between the central point and all other points in the circle are evaluated. A histogram of these distances is made to calculate the radial two-dimensional pair distribution function later.

The circles are necessary to avoid any bias from data points that lie in the corners of the square-shaped boxes. The density cut-off avoids bias from regions that are partially empty (e.g. by edges or projections during the capture time of the image).

Results

Fig. 3 shows a comparison between the measured distance distribution and the distance distributions one will get, if one puts the same number of particles into an identically shaped nucleus by random. The difference between the two curves comes mainly from the influence of the nucleoli.

In order to examine the chromatin nanostructure the radial two-dimensional pair distribution function $g_{2D}(r)$ was used.

The pair distribution function will be proportional to the conditional probability $p(r)$ of finding a marker at a distance r, if another one is sitting at the origin. It is normalized in a way that a value of one corresponds to the mean particle density of the system. That means unbound H2B histones which are also fluorescently labelled are not expected to contribute to any structural motif since they are assumed to be uniformly distributed all over the nucleus.

For this analysis the formerly described block analysis was used to find and cut out suitable spheres with a radius of 400 nm. Then all distances between the center and any other marker in each sphere are evaluated to calculate $p(r)$ and it was averaged over all possible spheres in a particular nucleus (i.e. $g_{2D}(r)$ is calculated by a histogram of $\approx 10^6 - 10^7$ distances). The centers of the spheres themselves were not considered. Thus, one gets one distribution function per nucleus.

The two-dimensional pair distribution function is given by

$$g_{2D}(r) = \left[\left(\frac{A}{N-1}\right)\frac{1}{\pi[2r\Delta r + \Delta r^2]}\right]\left[\frac{1}{N}\sum_{i=1}^{N}\sum_{j\neq i}\delta(r - r_{i,j})\right],$$

where Δr=10nm is the binning width for the histogram used to calculate $p(r)$, $(N-1)/A$ is the average particle density of the 400nm-sphere and N is the total number of particles the sphere contains. The factor $\pi[2r\Delta r + \Delta r^2]$ is just the area of a ring of width Δr with a mean radius of $r + \Delta r/2$.

The average pair distribution functions for HeLa and Fibroblast nuclei are shown in Fig. 4. One can clearly see that a chromatin nanostructure beyond the level of the nucleosome exists: $g_{2D}(r)$ is larger than one for distances below 150 nm which means that the nucleosomes are organized somehow.

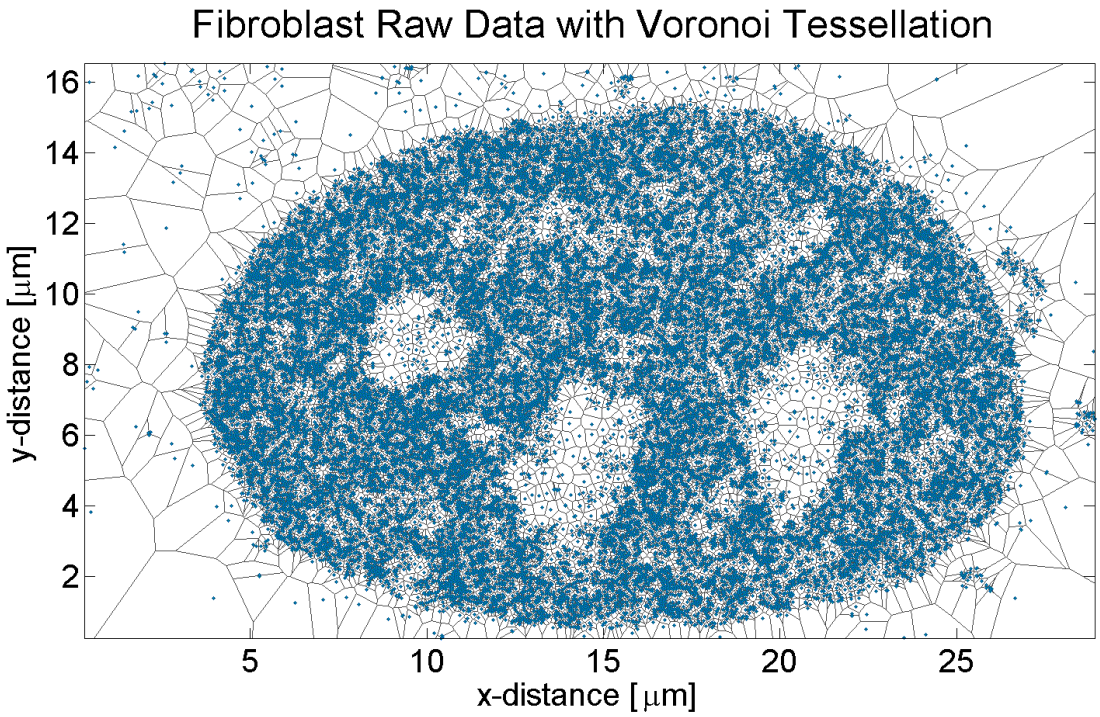

Figure 1: This figure shows a Voronoi diagram of the localization data. One can see that points that are close to each other have small Voronoi cell sizes, whereas other points that are trailed off have large cells. For this figure Fibroblast #27 was used.

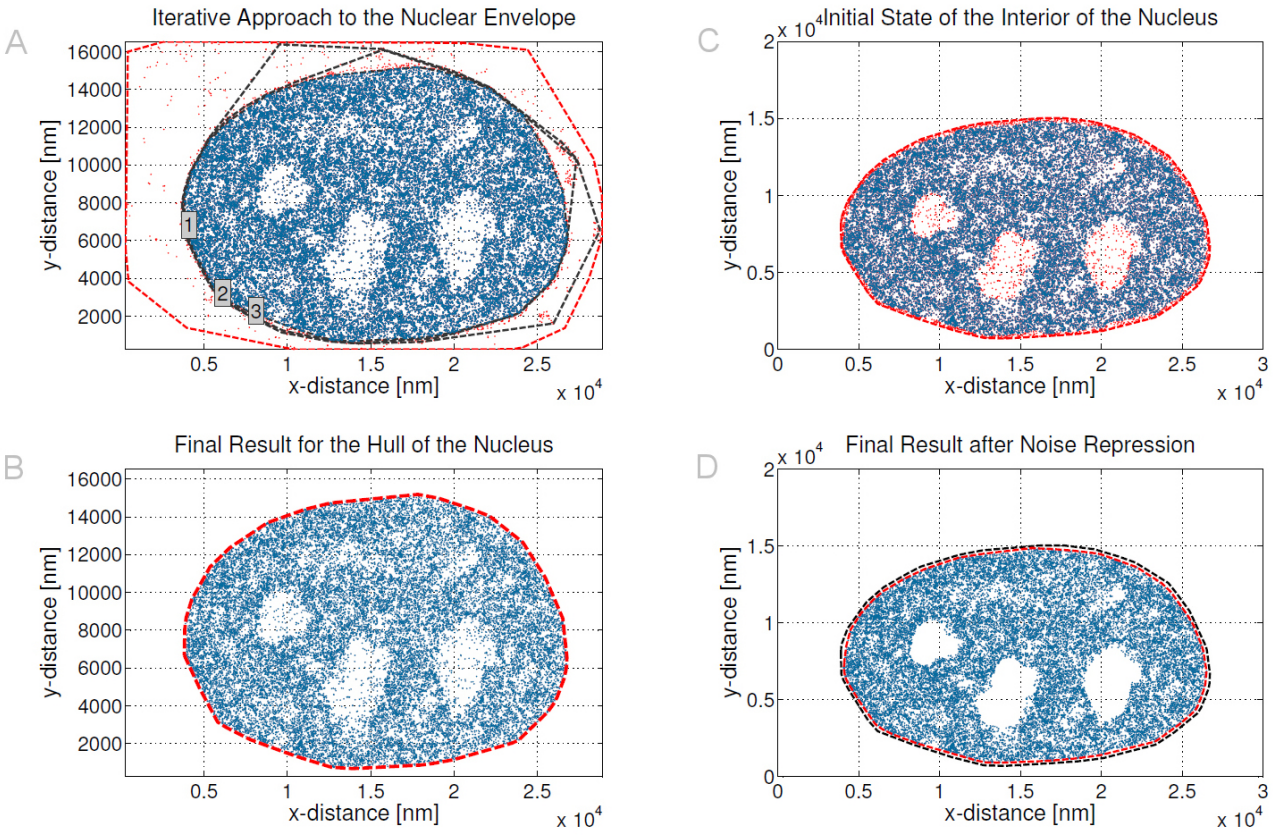

Figure 2: Noise repression with Voronoi tesselation. **A and B** An example of the determination of the convex hull of a Fibroblast nucleus. Iteratively, data points are sorted out which have a too large Voronoi cell size (cf. red dots). The different iterations are marked with the labels 1,2 and 3 (top). The convex hull after every iteration is shown as well (black dashed line). **C and D** This figure shows the noise reduction in the interior of a Fibroblast nucleus. Again Voronoi diagrams are calculated iteratively and data points with too large cell sizes are sorted out (cf. red dots) just like the heterochromatin.

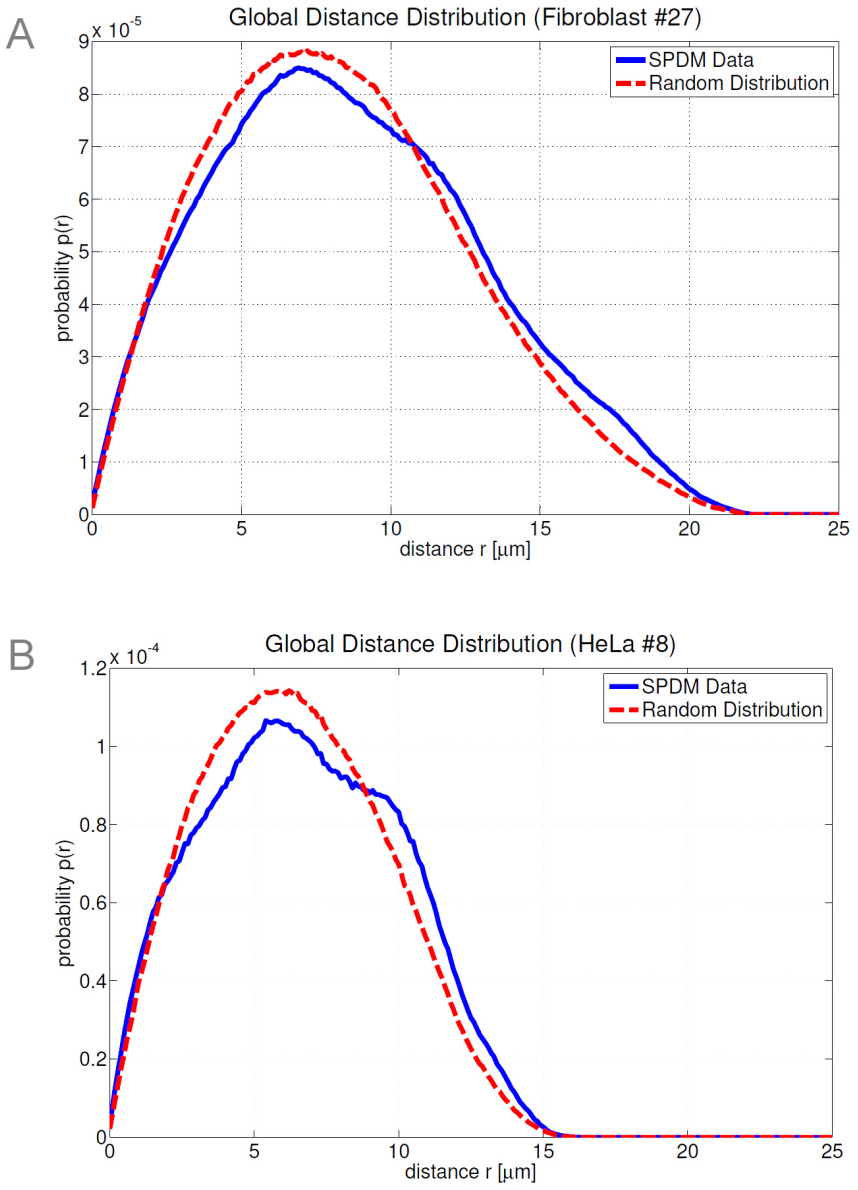

Figure 3: A comparison of a measured H2B distance distribution and a random particle distribution within an identically shaped nucleus. The differences come mainly from the influence of the nucleoli.

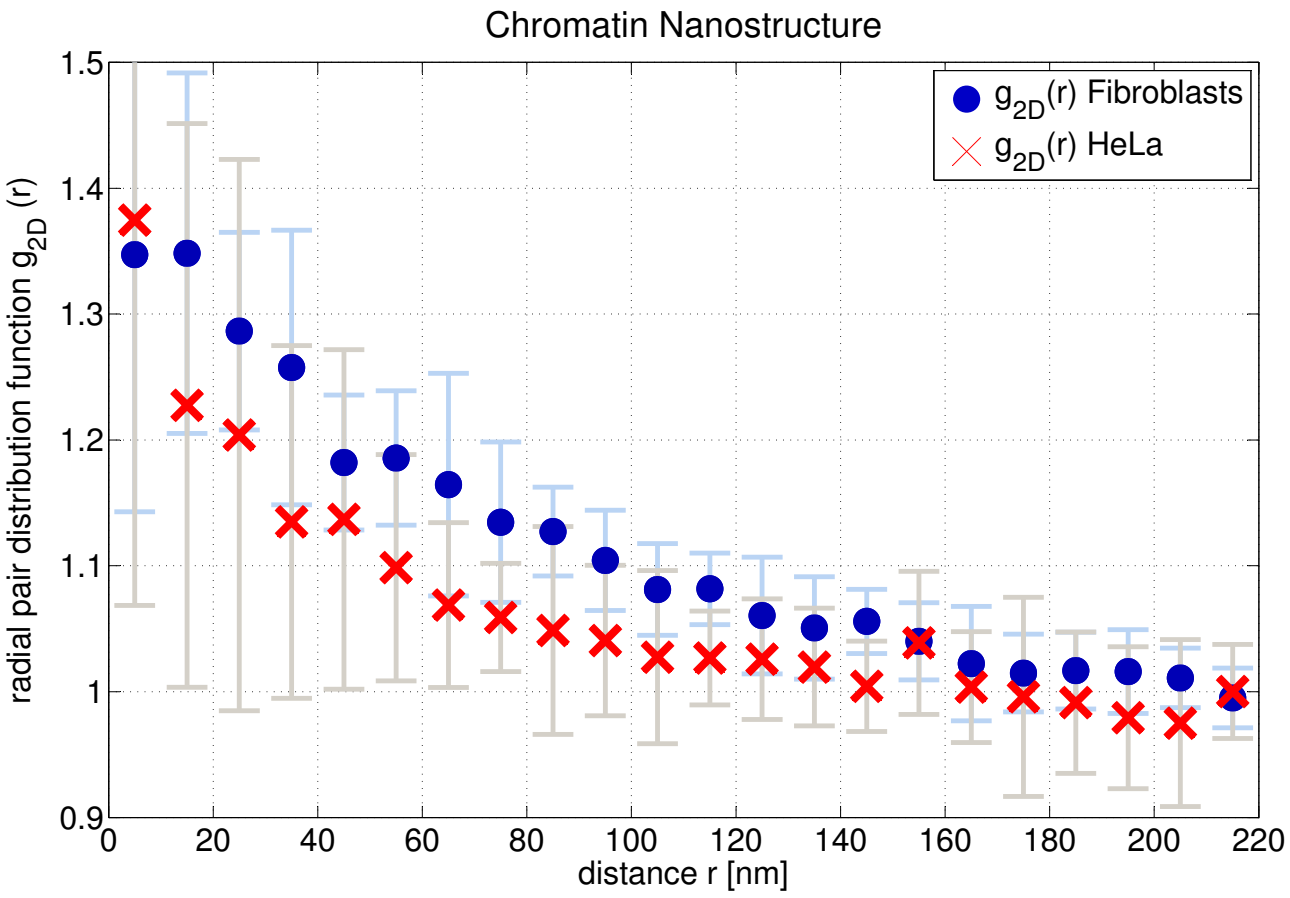

Figure 4: The radial two-dimensional pair distribution function describes the nanostructure of the emGFP-marked nucleosomes for the Fibroblasts and HeLa strain I. One can clearly see some structure beyond the scale of the nucleosome since $g_{2D}(r)$ is larger than one for small distances. The error bars indicate the cell-to-cell variation.

References

[1] Bystricky, K., P. Heun, L. Gehlen, J. Langowski and S. M. Gasser. 2004. Long-range compaction and flexibility of interphase chromatin in budding yeast analyzed by high-resolution imaging techniques. Proc. Natl. Acad. Sci. U S A. 2004 November 23; 101(47): 16495ï¿½16500.

[2] Julio Mateos-Langerak, Manfred Bohn, Wim de Leeuw, Osdilly Giromus, Erik M. M. Manders, Pernette J. Verschure, Mireille H. G. Indemans, Hinco J. Gierman, Dieter W. Heermann, Roel van Driel, and Sandra Goetze. Spatially confined folding of chromatin in the interphase nucleus. Proceedings of the National Academy of Sciences. February 2009.

[3] Yokota, H. M.J. Singer, G.J. van den Engh, and B.J. Trask. 1997. Regional differences in the compaction of chromatin in human G_0/G_1 interphase nuclei. Chromosome Res., 5:157–166.

[4] Poupon, A. (2004). Voronoi and Voronoi-related tessellations in studies of protein structure and interaction. Current Opinion in Structural Biology, 14(2), 233-241.

[5] Barry Boots, Atsuyuki Okabe, Kokichi Sugihara and Sung Nok Chiu. 2000. Spatial Tessellations: Concepts and Applications of Voronoi Diagrams (Wiley Series in Probability & Mathematical Statistics) Wiley & Sons, Second Edition.

[6] Bolzer, A. Gregor Kreth, Irina Solovei, Daniela Koehler, Kaan Saracoglu, Christine Fauth, Stefan Mï¿½ller, Roland Eils, Christoph Cremer, Michael R. Speicher, Thomas Cremer. Three-Dimensional Maps of All Chromosomes in Human Male Fibroblast Nuclei and Prometaphase Rosettes. 2005. PLoS Biol 3(5): e157 DOI: 10.1371/journal.pbio.0030157

[7] Barber, C. B., D.P. Dobkin, and H.T. Huhdanpaa, "The Quickhull Algorithm for Convex Hulls," ACM Transactions on Mathematical Software, Vol. 22, No. 4, Dec. 1996, p. 469-483. Available in PDF format at `http://www.acm.org/pubs/citations/journals/toms/1996-22-4/p469-barber/` and `http://www.qhull.org/`.

Supplementary Information 2: Analysis of the radial distribution function of a Lennard-Jones fluid.

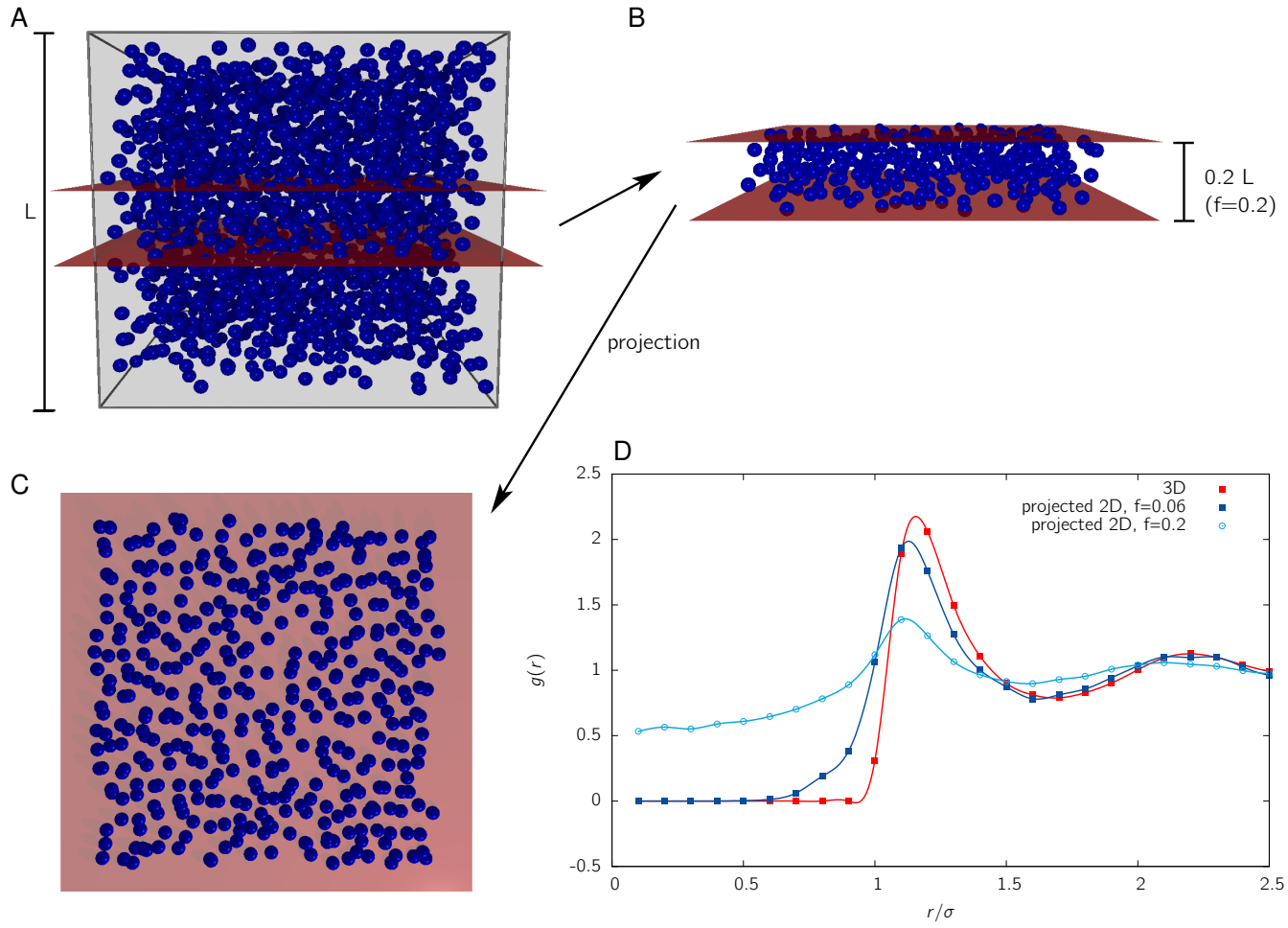

Figure 5: To analyze the effect of 2D projections on the radial distribution function $g(r)$, a three-dimensional Lennard-Jones system is simulated. Panel A displays an example conformation. As microscopy data provides a 2D projection of points comprising about 600 nm along the optical axis, a section is cut out of the simulation box (marked by the red plane). Panel B displays this section which is in this example 20% ($f = 0.2$) of the linear system size L. This data is then projected onto a 2D plane (panel C) and the radial distribution function is calculated. Panel D shows the results for the radial distribution function $g(r)$. The red curve displays the results for the 3D radial distribution function. It displays the typical behaviour: Below the hard-sphere radius of the fluid particles σ, no other particles can be found. The first peak corresponds to the first shell of molecules arranging close to each other due to the attractive interactions. Calculations are shown for a slice thickness of the slice of 6% and 20% of the linear system size. Assuming typical diameter of a human cell of about 10 μm, the optical section used in microscopy of 600 nm corresponds to the 6%-curve (fraction $f = 0.06$). Obviously, the projected radial distribution function still displays the structure-defining maxima and minima, although they are less pronounced. This analysis indicates that the projected rdf does not conceal structural information.

Supplementary Information 3: Simulations of chromosomes

Simulations of chromosomes are conducted using the Dynamic Loop model [2]. In this model, loop formation is achieved purely on the basis of diffusional motion. Each time, two chromatin segments randomly co-localize, a loop is formed with a certain probability. The loop attachment points dissolve again after some time, i.e. the lifetime of the loops is limited. Mapping histone distributions onto such a coarse-grained polymer model, requires the realistic time and length scales. We force the minimum distance between two chromatin segments to be 30 nm, corresponding to the presumed diameter of the chromatin fiber. As the bond flucutation model induces a minimum distance between two segments of 2/3 lattice units, 45 nm correspond to one lattice unit. The persistence length of chromatin is approximately $l_p = 150$ nm [3], the average length of one segment in the bond fluctuation model 2.71 lattice units, i.e. approx 122 nm. Thus, such a mapping requires introducing a bending rigidity, which is accomplished by the following potential for bond angles,

$$U_{\text{bond}} = \kappa_\theta(1 - \cos\theta)$$

Similar potentials have been used in Refs. [5, 1]. To establish a relationship between persistence length l_p and the potential parameter κ_θ, we conduct simulations of self-avoiding walks in a semi-dilute solution of occupancy fraction 10%. The density of chromatin is roughly 10% and this value has been used in other studies [4]. Simulations are run with different values of κ_θ and the angular correlations $\langle\cos\theta\rangle$ of neighbouring bonds are calculated. The relationship bewteen the potential parameter κ_θ and the angular correlation is shown in Fig. 6. A realistic chromatin model requires that $\langle\cos\theta\rangle = \exp(-l/l_p) = \exp(-2.71 \cdot 45\text{nm}/150\text{nm}) \approx 0.44$, yielding an interaction strength of $\kappa_\theta = 1.34$.

While simulations are conducted with a very low level of coarse-graining, it becomes intractable to simulate whole chromosomes. This, however, probably does not have a major impact on the structure at the level of single histones. Simulations are performed in a system of size $L^3 = (2.88\mu\text{m})^3$ and a density of $\rho = 0.1$. 27 chains of length $N = 256$ are put inside the simulation box.

To compare simulational results with localization microscopy data, histones have to be distributed along the simulated chromosomes. The linear dimension of $L = 64$ l.u. corresponds to 2.88 μm. Experimental data evaluation is done in a 2D projection of a slice of thickness $d = 600$ nm. The average density of localized histones has been determined to about $150/\mu\text{m}^2$. In order to obtain a similar density for simulated fibers, $K = 5971$ histones are randomly distributed along the contour of the chromosomes. To mimic the effect of the thickness of the chromatin fiber, each point is shifted randomly within a radius of 15 nm in the plane perpendicular to the chromatin fiber. Furthermore, excluded volume effects are taken into account by not allowing two virtual fluorophores be closer than 5 nm, the estimated radius of a nucleosome [6]. An example conformation of the system is shown in Fig. 7A. The distribution of histones is visualized in Fig. 7B. The chromosomes are shown as small red threads, the simulated localized fluorophores are marked by green points. After distributing histones along the simulated chromosomes, a z-slice of thickness 600 nm is cut out of the simulation box (Fig. 7C) and all histones inside this slice are projected onto the xy-plane (Fig. 7D). This projected data is then analyzed the same way as the experimental data, i.e. the block distribution analysis is conducted.

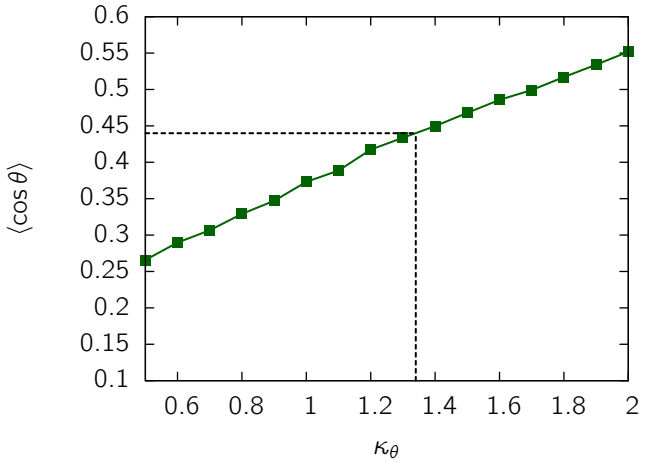

Figure 6: Relation between the bond-angle potential $U_{\text{bond}} = \kappa_\theta(1-\cos\theta)$ and the persistence length for linear chains using the bond-fluctuation algorithm. Shown are simulational results of a system with density $\rho = 0.1$ and linear system size $L = 64$ lattice units. The parameter κ_θ was varied and the resulting average bond angle between neighbouring bonds $\langle\cos\theta\rangle$ was calculated. At $\kappa_\theta = 1.34$ the potential resembles the biological case where the persistence length is 150 nm.

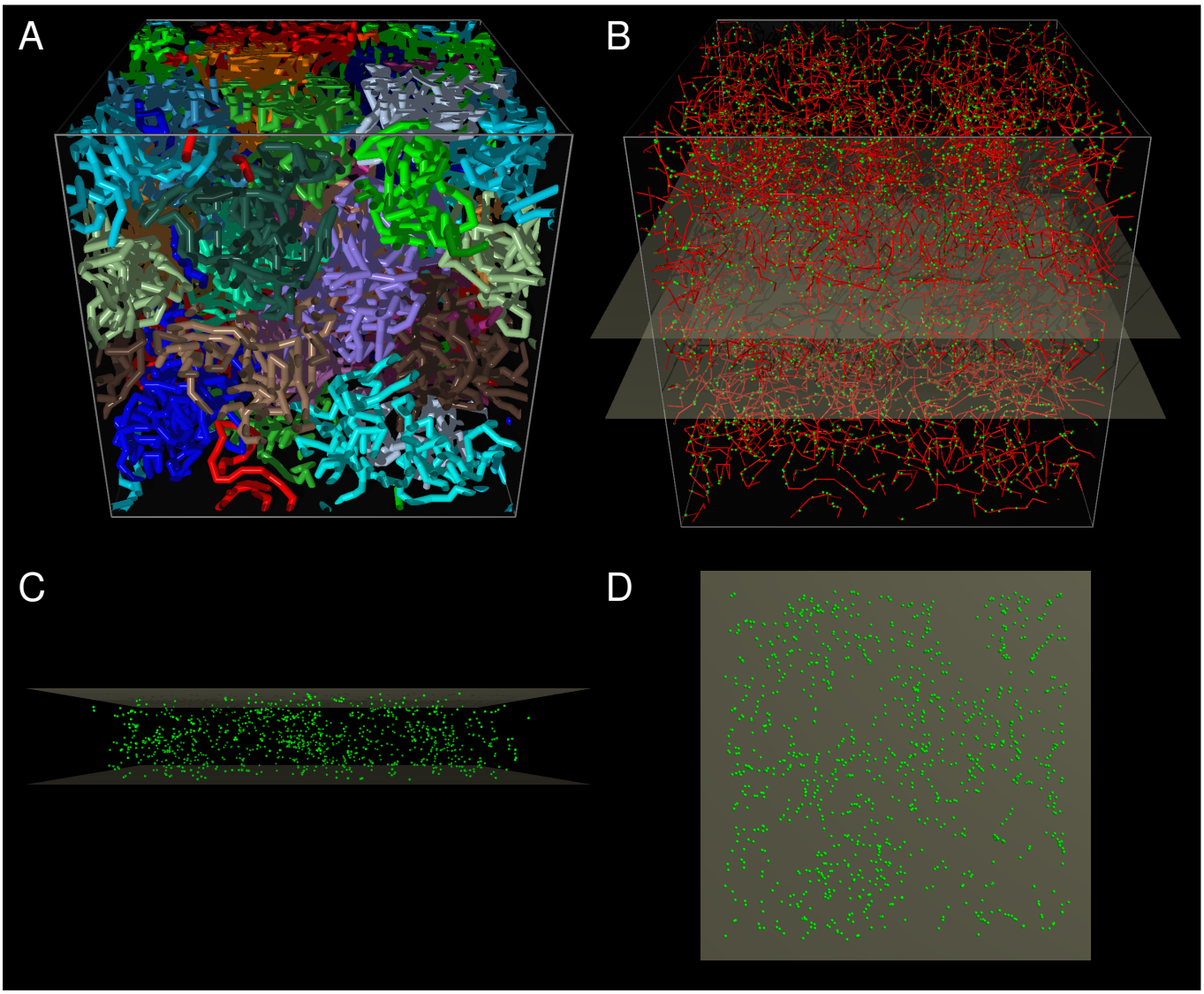

Figure 7: Histone distribution and projection for simulated chromosomes (Dynamic Loop Model). **A.** Example conformation with several chromosomes in the simulation box. Simulations are set up with an average number of loops per monomer of 0.32. **B.** Distribution of localized histones along the fibers (green points). The red threads mark the path of the chromosomes, the two planes have a distance of 600 nm. **C.** A slice of thickness 600 nm is cut out of the simulation box. **D.** The localized histones inside this slice are then projected onto the plane for conducting the block analysis.

References

[1] Rolf Auhl, Ralf Everaers, Gary S. Grest, Kurt Kremer, and Steven J. Plimpton. Equilibration of long chain polymer melts in computer simulations. *The Journal of Chemical Physics*, 119(24):12718–12728, 2003.

[2] Manfred Bohn and Dieter W. Heermann. Dynamic looping of chromatin: A diffusion-based polymer model with probabilistic loops. *submitted to PLoS Computational Biology*, -:–, 2009.

[3] Kerstin Bystricky, Patrick Heun, Lutz Gehlen, Jörg Langowski, and Susan M Gasser. Long-range compaction and flexibility of interphase chromatin in budding yeast analyzed by high-resolution imaging techniques. *Proceedings of the National Academy of Sciences of the United States of America*, 101(47):16495–16500, Nov 2004.

[4] Peter R. Cook and Davide Marenduzzo. Entropic organization of interphase chromosomes. *J. Cell Biol.*, 186(6):825–834, 2009.

[5] Angelo Rosa and Ralf Everaers. Structure and dynamics of interphase chromosomes. *PLoS Computational Biology*, 4(8):e1000153, 2008.

[6] H. Schiessel, W. M. Gelbart, and R. Bruinsma. DNA folding: structural and mechanical properties of the two-angle model for chromatin. *Biophysical Journal*, 80(4):1940–1956, Apr 2001.